**2.4 FRACTURE BEHAVIOR OF ADVANCED ODS ALLOY 9YWTV –** T. S. Byun, D. T. Hoelzer (Oak Ridge National Laboratory), J. H. Yoon (Korea Atomic Energy Research Institute), and S. A. Maloy (Los Alamos National Laboratory)

## OBJECTIVE

Nanostructured ferritic alloys (or advanced ODS alloys) have been considered as primary candidate materials for fusion reactors because of their excellent high temperature creep strength and irradiation resistance. This research aims at characterizing and understanding the fracture behaviors of newly developed 9YWTV alloy with improved fracture toughness.

## SUMMARY

Latest studies on the high temperature fracture of nanostructured ferritic alloys (NFAs) have indicated that the microcracks formed within the alloys propagate by a low energy boundary decohesion mechanism and therefore resulted in low fracture toughness. A 9Cr NFA with improved fracture toughness was successfully developed by applying thermo-mechanical treatments (TMTs) designed to enhance grain boundary bonding. This article focuses on the static fracture behaviors of the newly developed 9Cr NFAs. Fracture mode and cracking resistance were compared among the materials treated through different controlled rolling (CR) routes. Optimal TMTs resulted in high fracture toughness at room temperature (> 250 MPa√m) and in retaining higher than 100 MPa√m over the wide temperature range 22–700°C. Significant differences were found in the fracture resistance (J-R) curves among the low and high fracture toughness NFAs.

## PROGRESS AND STATUS

### Introduction

In the past decade, the nanostructured ferritic alloys (NFAs) with ultra-high strength (1–2 GPa) have been developed for various nuclear reactor applications such as the first-wall structure of gas-cooled fusion reactors and advanced sodium-cooled fast reactor for their excellent high temperature creep strength and high dose irradiation resistance [1-13]. One of the major issues that we inevitably face in developing such ultra-high strength materials is the resulting low toughness and low ductility. However, although high initial toughness and ductility are essential for preventing cracking for both manufacturing and delaying the onset of radiation-induced embrittlement, this key engineering requirement has not been a focus of development efforts in major research programs. A series of studies of deformation and fracture mechanisms using 14YWT NFA indicate that the microcracks tend to propagate along grain boundaries without significant plastic deformation, resulting in low energy grain boundary decohesion and low fracture toughness [14-22].

It has been proposed that strengthening grain bonding could be achieved through thermo-mechanical treatments (TMTs) specially designed to enhance grain boundary inter-diffusion [22]. Recently, 9Cr NFAs with high toughness have been successfully developed by applying optimum TMTs to as-consolidated NFAs [15-25]. Since a proper fracture resistance is a key requirement for any engineering grade material, the purpose of the detailed study on the newly developed 9Cr NFAs was set to elucidate and characterize the static fracture behaviors focusing on high temperature fracture resistance and mechanism.

In search of high fracture toughness conditions, two series of TMTs, i.e., isothermal annealing and controlled rolling treatments, have been applied to two as-extruded NFAs with normal chemistry of Fe(bal)-9Cr-2W-0.4Ti-0.2V-(0.05 and 0.12)C-0.3$Y_2O_3$ [24]. These different TMTs were supposed to produce widely different fracture behaviors. A three-point bar (TPB) type miniature fracture specimen with dimensions of 15 mm×5 mm×2.5 mm (thickness) was used for static fracture (J-R) testing. Fracture

tests on the miniature TPB specimens have been performed at 22 – 700 °C at a nominal gage speed of 0.05 mm/min [26-32]. Process dependence of J-R curve and fracture toughness is the focus of discussion in this article. Fracture test result showed that some optimum TMTs resulted in fracture toughness similar to those of conventional quenched and tempered ferritic-martensitic steels. Fracture surfaces and J-R curves are compared to find the origin of such a significant improvement in fracture toughness.

**Experimental**

Base materials and thermomechanical treatments

Two new Fe-9Cr nanostructured alloys have been developed to improve fracture toughness by integrating the best practices in the mechanical milling-based steel-making technology. Details of the integrated processing technology can be found in earlier publication [33] and a summarized description is provided here. The alloy powders were produced in the ATI Powder Metals Co. in Pittsburgh, PA, using an integrated process of vacuum induction melting and argon gas atomization. The product chemistries of the two Fe-9Cr-alloy powders were Fe-8.84Cr-2.04W-0.38Ti-0.21V-0.05C (heat L2476) and Fe-9.02Cr-2.11W-0.38Ti-0.21V-0.11C (heat L2477), which correspond to 10% and 11.5% Cr-equivalents, respectively. The yttrium oxide ($Y_2O_3$) powder to be mixed with these alloy powders for mechanical milling was purchased from the Nanophase Technology Co. and has particle sizes ranging from 17 to 31 nm.

In the production of NFAs, the mechanical milling process is designed to provide a completely-alloyed status of the material without any precipitation or evident elemental segregation. The two alloy powders have been mechanically-milled in Zoz GmbH CM08 attritor milling machine after being mixed with 0.3 wt.% yttrium oxide ($Y_2O_3$) powder. Each of the loads for milling comprised 997 g of an alloy powder and 3 g of $Y_2O_3$ powder and was milled for 40 hours in static argon environment in water cooled chamber. For consolidation, the mechanically-alloyed powders were filled into mild steel cans with 50 mm inner diameter and evacuated to a vacuum of ~1 Pa at ≤ 400 °C. The consolidation process, i.e., hot extrusion operation, was performed in the Watson-Stillman unit at ORNL with a capacity of 1.25 kilotons. During the extrusion operation a peak force of ~900 tons was taken to extrude a 90 mm (outer) diameter can containing ~1 kg mixed powder. The two as-extruded NFAs were designated as 9YWTV-PM1 (with higher carbon) and 9YWTV-PM2 (with lower carbon). Up to this step, the processing details were the same as those developed for 14YWT [27].

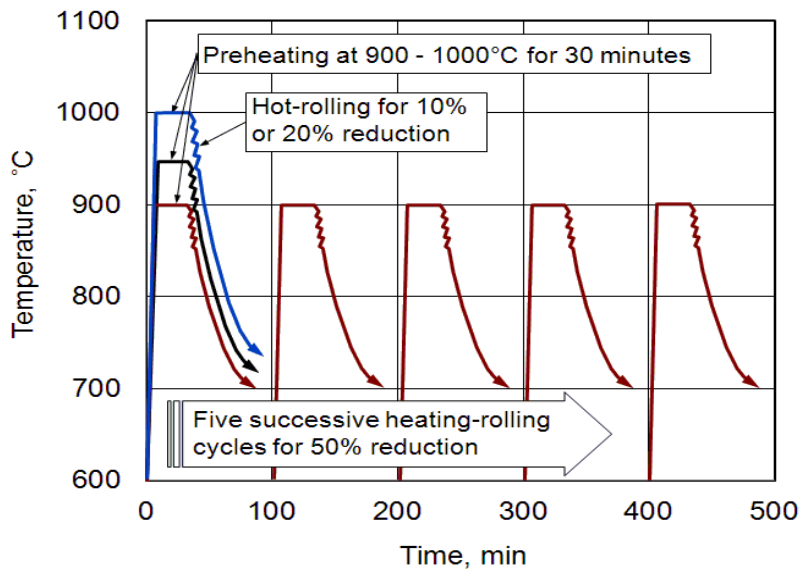


**Figure 1.** Controlled rolling (CR) processes applied to 9Cr NFAs [33]. Note that the 20% reduction was made by one-step rolling and the 50% rolling was made by five 10% reductions and that the rolling temperatures are believed to be close to the annealing (or rolling initiation) temperatures as the coupons were still cladded with 4–6 mm thick mild steel (can material).

The final processing step was controlled rolling (CR) or repeated rolling treatment in two-phase temperature region: the as-extruded or base NFAs were controlled-rolled at 900, 925, 950, 975, and 1000 °C for 20 or 50% total reduction (i.e., isothermally annealed and rolled down on cooling in air). The hot-rolling treatments have been applied to ~5 cm long coupons after heating to 900–1000 °C for 30 minutes; this temperature range was chosen considering the temperature range for α to γ transformation (850–1000°C), hot formability of NFAs (> ~900°C), and prevention of abnormal grain growth (< ~1100°C) [33]. Since the coupons were still cladded by the mile steel can material and thus cooling in the meat NFA was limited during the rolling, the actual rolling temperatures for the NFAs were believed to be very close to the specified ones in 900 – 1000 °C. Figures 1 illustrates schematic routes of CR treatments applied to the two base NFAs.

Specimen preparation

For the two NFAs treated in various conditions, static fracture testing was performed in an MTS servo-hydraulic testing machine with a vacuum furnace at select temperatures in the range of 22(room temperature)–700 °C using miniature bend bar specimens with nominal dimensions of 15 mm in length and 5 mm in width and 2.5 mm in gross thickness. These specimens had a 1.5 mm long wire-cut notch and 0.25 mm deep side groove in each side, as illustrated in Figure 2. All specimens had L-T orientation, in which the loading direction is in the extrusion direction and crack extension occurs in the perpendicular direction. Prior to the fracture testing, precracking to produce sharp crack tip was carried out for each specimen under a nominal cyclic load of at 500 ± 450 N at 20 - 30 Hz. Precracking was made until the machined notch (1.5 mm) extended by 0.5–1.2 mm; the nominal crack length-to-specimen width ratio (a/W) was about 0.46 after the precracking.

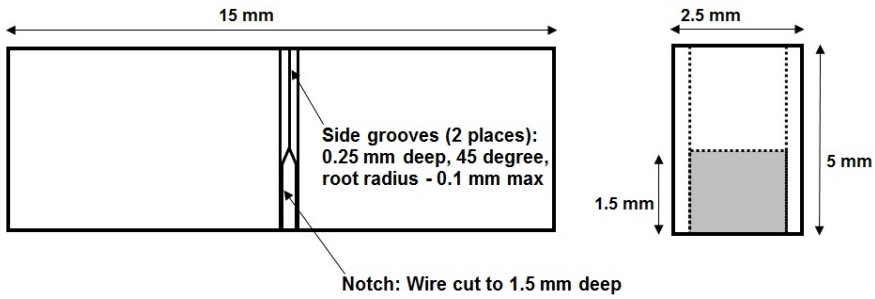


**Figure 2.** Dimensions of three-point bend bar fracture specimen.

Static fracture resistance (J-R) testing and analysis

Fracture resistance (J-R) tests in quasi-static mode were carried out at a crosshead speed of 0.005 mm/s with a temperature control within ±1$^{o}$C. For each TMT condition, 2 - 7 J-R tests were conducted at select temperatures of 22, 200, 300, 400, 500, 600, and 700°C and in a vacuum of ~$10^{-4}$ Pa (~$10^{-6}$ torr), except for the room temperature (22°C) tests in air. Each specimen was soaked at a desired temperature for 5 – 10 minutes prior to the initiation of each J-R test. All of the J-R fracture tests were run in a displacement-controlled three-point bending mode, and the static fracture testing and evaluation were performed following the standard procedure described by the ASTM Standard E1820-09, Standard Test Method for Measurement of Fracture Toughness. As the normalized method was applied to the construction of fracture resistance (J-R) curves, the monotonic load-displacement curves without loading-unloading cycles were recorded. In each test loading was stopped when the load decreased to about 50% of maximum load or a catastrophic failure occurred before the 50% load point. After each J-R test, the tested specimen was fatigue-loaded in air to make a mark for the final crack length before the complete separation of the specimen. The initial and final crack lengths were then measured optically. Figure 3 displays examples for the optical photographs of fracture surface, in which the white portions were formed by high cycle fatigue loading and provides easily discernible crack surface regions. The dark area between the lower and higher white areas is the surface formed by the stable fracture testing. The Figure 3(a) is an exception that has experienced brittle failure [35-42].

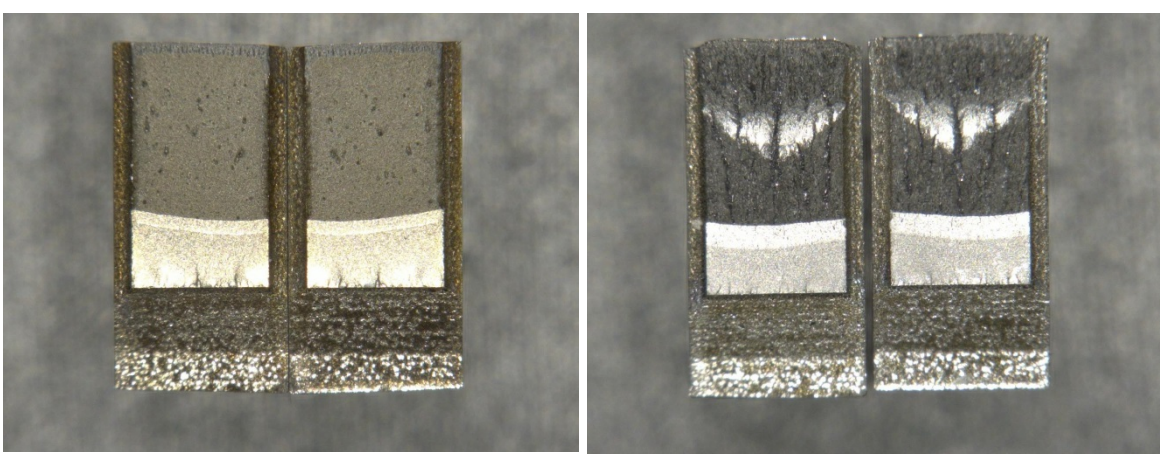

**(a) 9YWTV-PM1 as-extruded, tested at 600 $^{o}$C** **(b) 9YWTV-PM2 as-extruded, tested at 200 $^{o}$C**

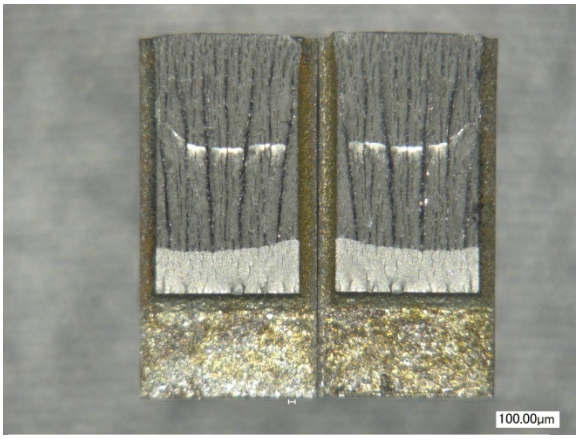


**(c) 9YWTV-PM1 50% rolled at 1000 °C, tested at RT**

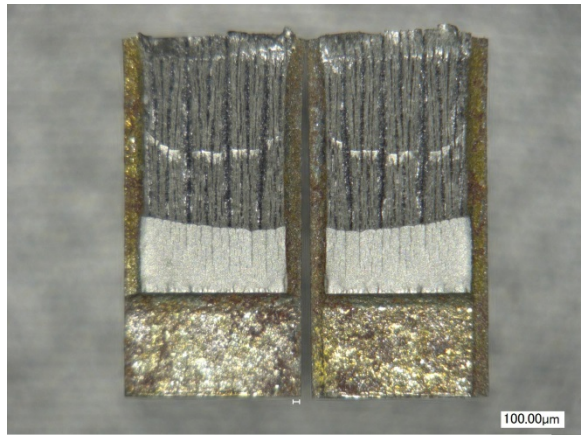


**(d) 9YWTV-PM2 50% rolled at 1000 °C, tested at RT**

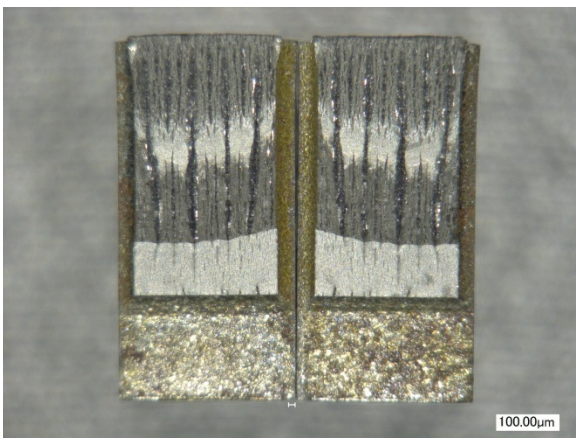


**(e) 9YWTV-PM2 50% rolled at 975 °C, tested at RT**

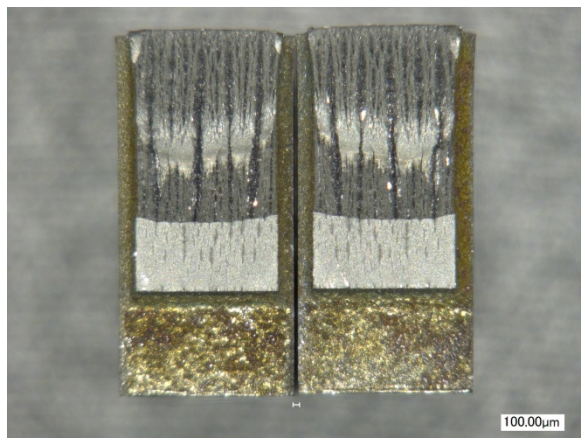


**(f) 9YWTV-PM2 50% rolled at 975 °C, tested at 500 °C**

**Figure 3**. Examples for the optical photographs of fracture surfaces. The white portions are from fatigue loading, which were used for crack length measurement.

In the data analysis procedure to construct the J-Resistance curve (or J-integral versus Δa curve), the crack growth values were obtained using the normalization curve method. This simplified J-R curve calculation method is described in the ASTM Standard. To use the normalization curve method, two datasets need to be obtained: a load-displacement curve of up to ~50% of the maximum load, and the initial and final crack lengths, both of which were obtained during testing and microscopy as aforementioned. For each J-R curve, the interim fracture toughness value ($J_Q$) is determined at the intersection of the J-R curve and the 0.2 mm offset line of the blunting line using the formula and procedure described in the ASTM standard [34]. The final fracture toughness data are also given in the form of stress intensity factor, $K_{JQ}$, which can be converted from the $J_Q$ data using the following relationship:

$$K_{JQ} = \sqrt{J_Q E/(1-\nu^2)} \qquad (1)$$

where E is the Young's modulus at given temperature (T in °C) (=218 – 0.045T-0.0001T$^2$ GPa) and v the Poisson ratio (=0.28, assumed temperature-independence).

It is worth noting that the fracture toughness data ($K_{JQ}$) produced in this study remain as interim values ($K_{JQ}$) because the curvature at crack frontline and the limitation imposed by small specimen volume and thickness cannot satisfy some of the standard requirements for the validation towards formal fracture toughness ($K_{IC}$). It is also important to note that the standard practice used leads to an overestimation when small specimens are used [43-48]. Such overestimation originates from application of the standard practice of using the 0.2 mm shifted crack blunting line to the different uncracked ligaments: the present miniature TPB specimen has a nominal uncracked ligament of ~2.5 mm, which is very small compared to any types of standard fracture specimens. As indicated in Figure 3, the excessive plasticity or loss of stress constraint, which is often observed in soft material miniature specimens, is not a cause for the overestimation.

**Results and discussion**

Characteristics of fracture resistance (J-R) behavior

A J-integral versus $\Delta a$ curve, which is obtained from load-displacement data using either curve normalization method or unloading compliance method, can represent the fracture resistance (J-R) of an alloy during crack growth. Cracking resistance at or near the initiation is usually defined as fracture toughness ($J_{IC}$ for example) and is considered as the most important fracture parameter, however, the slope and height of the J-R curve after the initial portion can also be useful in characterizing overall cracking resistance of the material as a growing crack tends to stop earlier with higher J-value. This section compares the J-R curves of the two 9Cr NFA materials in various conditions.

The J-R curves in as-irradiated condition are compared in Figure 4. First of all, it is noted in this figure that four of eight J-R curves are buried in the initial linear line (blunting line) as those specimens have fractured in either linear elastic or crack blunting region. It is worth remembering that such buried lines exist in the following plots. Among the J-R curves with crack extension, the 9YWTV-PM2 alloy tested at low temperatures, room temperature and 200 $^{o}$C, displayed strong fracture resistance. However, the other two curves obtained from high temperatures, 9YWTV-PM1 at 500 $^{o}$C and 9YWTV-PM2 at 700 $^{o}$C, showed much lower resistance. As these base NFA specimens fracture without crack growth or experience crack growth at a low resistance, resulting fracture toughness at a high temperature ≥ 500 $^{o}$C seems to be as low as those of the reference material 14YWT-SM10 [33].

At room temperature, the 9YWTV-PM2 alloy after CR displays much higher fracture resistance when compared to the base material, Figure 5. The two J-R curves of 9YWT-PM2 after 900 $^{o}$C rolling show extraordinary long blunting lines, from which high fracture toughness values are measured as they are determined at maximum. In such cases with long blunting lines, the contribution of high strength to fracture toughness ($J_Q$) becomes significant. The other two curves of 9YWTV-PM2 alloy after CR at 975 and 1000 $^{o}$C display high J-values with relatively high slopes (dJ/da). It is obvious that the 9YWTV-PM1 alloy has relatively lower fracture resistance as the two J-R curves after 975 and 1000 $^{o}$C CR are located lower than those of 9YWTV-PM2 alloy and the specimens after 900 $^{o}$C CR have failed without stable crack growth and curves are buried in linear portion.

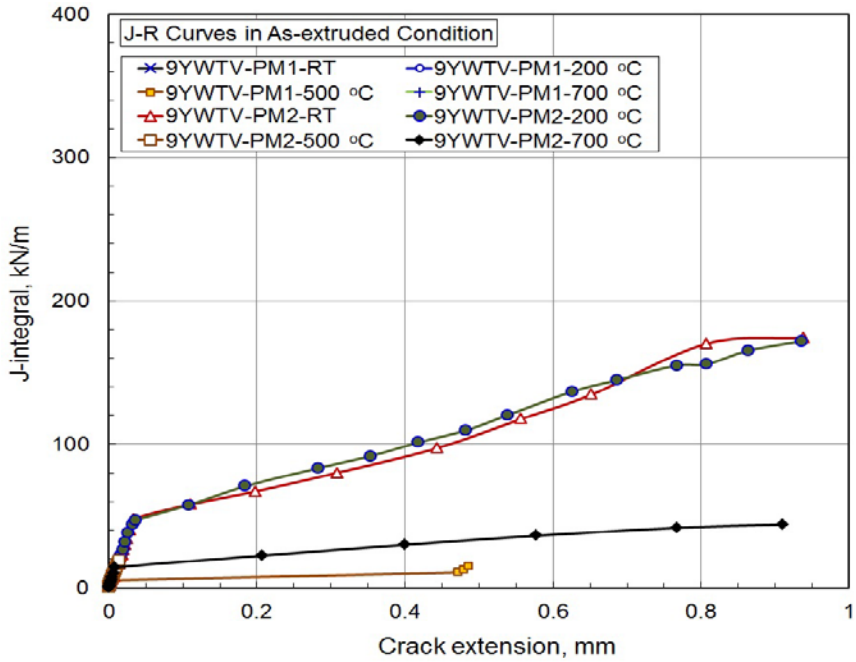


**Figure 4.** J-R curves from the miniature bend specimens of 9YWTV-PM1 and -PM2 in as-extruded condition.

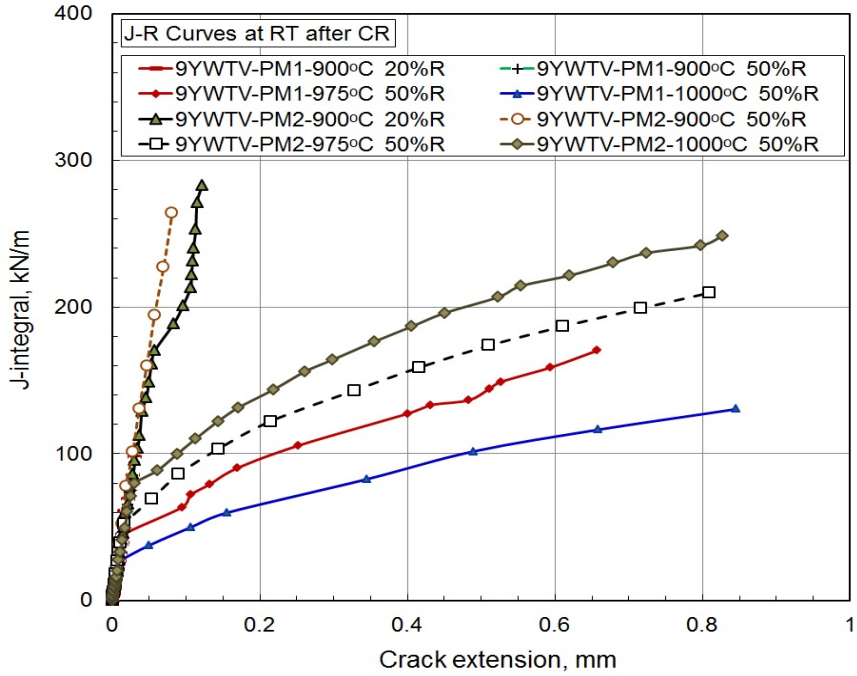


**Figure 5.** J-R curves from the miniature bend specimens of controlled rolling (CR) treated 9YWTV-PM1 and -PM2 tested at room temperature.

High temperature fracture resistances are compared in Figures 6 and 7. The J-R data in Figure 5 indicate fracture resistance is relatively higher at 500 °C than at 700 °C. There are also exceptions: in the two cases of 9YWTC-PM1 after CR at 900 °C, the all J-values contained on the blunting line. Meanwhile, as seen in the room temperature data, the 9YWTV-PM2 after CR at 900 °C has noticeably higher fracture resistance compared to the other alloy or CR conditions.

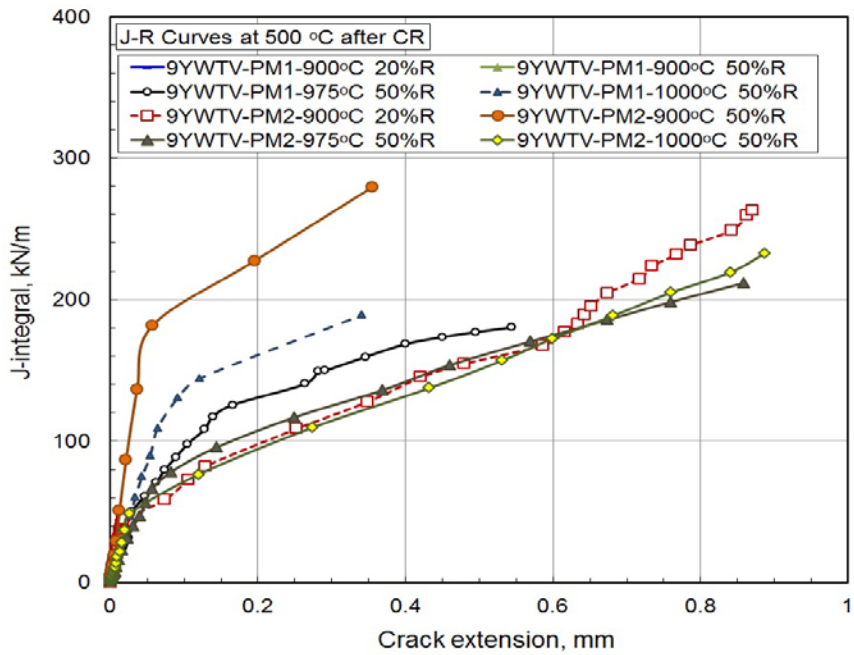


**Figure 6.** J-R curves from the miniature bend specimens of controlled rolling (CR) treated 9YWTV-PM1 and -PM2 tested at 500 °C.

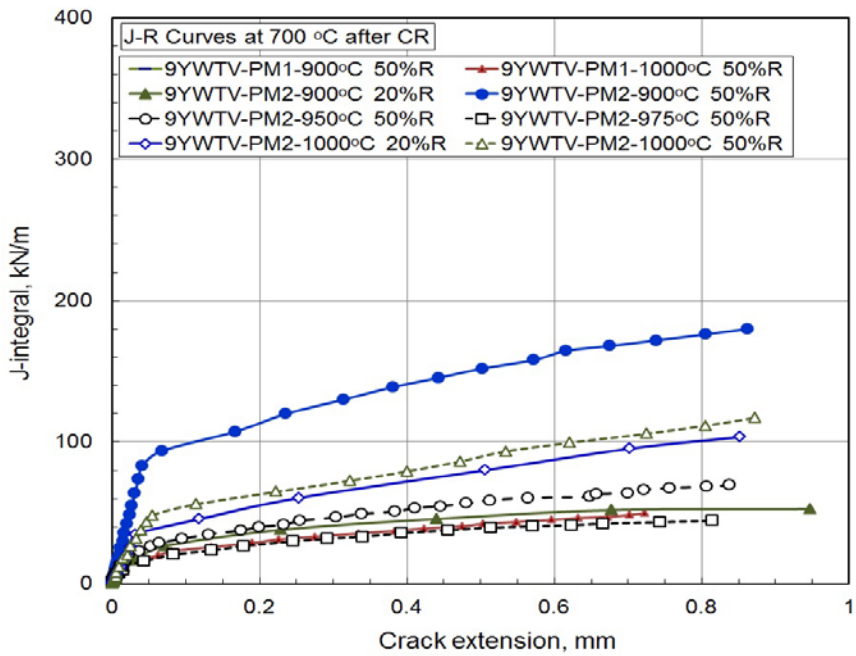


**Figure 7.** J-R curves from the miniature bend specimens of controlled rolled 9YWTV-PM1 and -PM2 tested at 700 °C.

For both materials, relatively lower fracture resistances were measured at 700 °C as illustrated in Figure 7. The higher carbon alloy 9YWTV-PM1 yielded low fracture resistance as the specimen after 900 °C CR has failed in brittle mode, and the J-R curve after CR at 1000 °C runs low although crack growth was stable. It is confirmed again that the 9YWTV-PM2 after CR at 900 °C has highest fracture resistance in the two materials in different TMT conditions.

Temperature dependence of fracture toughness ($K_{JQ}$)

In earlier publication [33] fracture toughness ($K_{JQ}$) data obtained at room temperature and 500 °C were used to determine effective TMT conditions that can produce high toughness NFAs. In Figures 8 and 9 the temperature dependence of $K_{JQ}$ over a wide range of temperature up to 700 °C is discussed for the CR treated NFAs. In the background the $K_{JQ}$ values of ferritic-martensitic (FM) steels, HT9 (12Cr-1MoWV) and NF616 (9Cr-2WVNb), are displayed in the upper band (colored light pink) and those of two 14YWTs and two base 9Cr NFAs are in the lower band (light blue). These datasets in two distinctive bands are used as benchmark data for improvement as the ultimate goal of this research was to develop a 9Cr NFA with fracture toughness comparable to those of the melting-based FM steels.

As displayed as the upper band, the $K_{JQ}$ of FM steels is typically in the range of 200 – 300 MPa√m at room temperature. Room temperature is believed to be in the upper shelf region of fracture toughness, and the ductile-brittle transition temperature (DBTT) of typical quenched and tempered FM steel is below room temperature [12]. Above room temperature the fracture toughness of FM steels slowly decreases with test temperature. The band widens, to a 100 – 260 MPa√m range at 700 °C because the $K_{JQ}$ difference between the toughest NF616 and the classic HT9 grows with temperature. Meanwhile, the $K_{JQ}$ data of 14YWTs and base 9YWTVs fall within the band of lower fracture toughness. Up to ~200 °C 14YWT-SM10 and 9YWTV-PM2 in as-extruded condition have 100–140 MPa√m, however, between 200 and 300 °C the $K_{JQ}$ for those NFAs dropped to well below 100 MPa√m, about a half of the peak toughness, and remained at the level in the range of 300–700 °C. Others, 14YWT-SM11 and 9YWTV-PM1 in as-extruded condition, show even lower toughness within the band.

In Figure 8 the $K_{JQ}$ values of 9YWTV-PM1 alloy after various CR treatments, larger data markers, are compared to the back ground data. For the majority of the data for CR-treated 9YWTV-PM1, the treatment did not help to improve fracture toughness. The only exception was the case of 975 °C CR treatment, which resulted in high fracture toughness in 100–600 °C span. A maximum toughness of ~240 MPa√m was measured in the 200–300 °C region and it decreased with temperature above 300 °C. The increase of $K_{JQ}$ in the RT–300 °C region may be considered as a toughness transition region, if not data scattering. Also, this standing out case with high $K_{JQ}$ over entire test temperature range is believed to be as an experimental error resulting from an inhomogeneity in material sampling; but further examination needs to be made for confirmation. Temperature dependence behaviors after 900 and 1000 °C CR-treatments are close to those of the low toughness back ground data.

As displayed in Figure 9, the improvement of fracture toughness by CR treatments is significantly more pronounced and consistent in the 9YWTV-PM2 alloy. The room temperature $K_{JQ}$ values were in the range of 150–280 MPa√m and the CR-treated PM2 alloy retained similar level of fracture toughness up to at least 300 °C. Obvious decrease with temperature started above 300 °C, but the sudden decrease of fracture toughness in 200– 300 °C region, which is often observed in high strength NFAs, did not occur in the CR-treated 9YWTV-PM2. At the highest temperature of 700 °C the $K_{JQ}$ value after 20% rolling at 900 °C and 50% rolling at 900 °C decreased slightly below 100 MPa√m. Except for a few data points at room temperature and 700 °C, the fracture toughness data of the CR-treated 9YWTV-PM2 fall within the band of FM steels. Overall temperature dependence of these CR-treated NFAs is also similar to that of FM steels.

Among the CR-treatments the 50% rolling at 900 °C demonstrated the highest fracture toughness, which retained high $K_{JQ}$ of >150 MPa√m over the entire test temperature range. The main reason for such high toughness is believed to originate from its high strength combined with appropriate ductility [45-49].

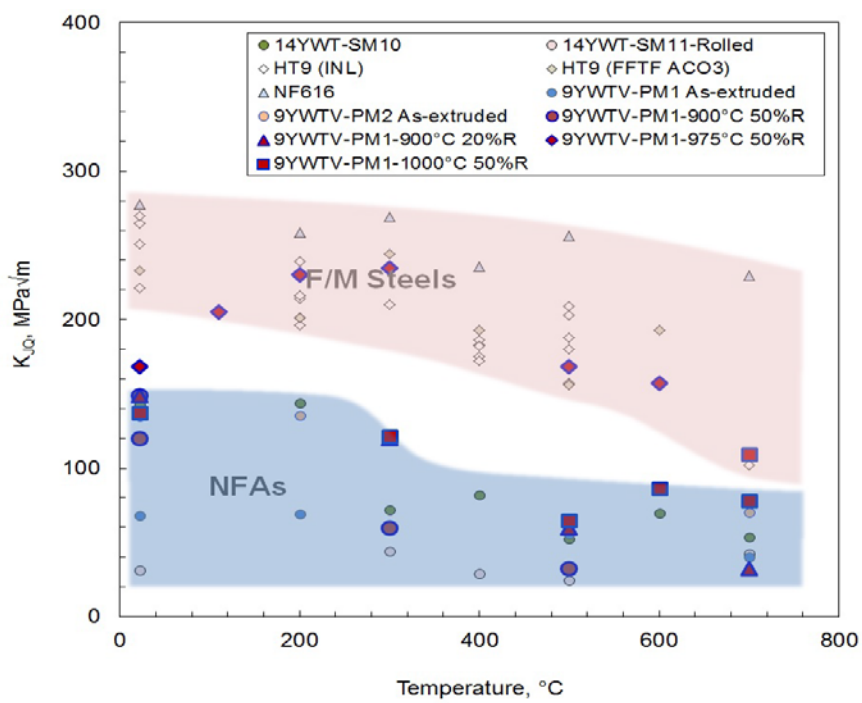


**Figure 8.** Temperature dependence in the fracture toughness ($K_{JQ}$) of 9YWTV-PM1 controlled rolled at various conditions. Data are compared with those of FM steels in pink (upper) shadowed area and those of lower toughness NFAs in blue (lower) shadowed area.

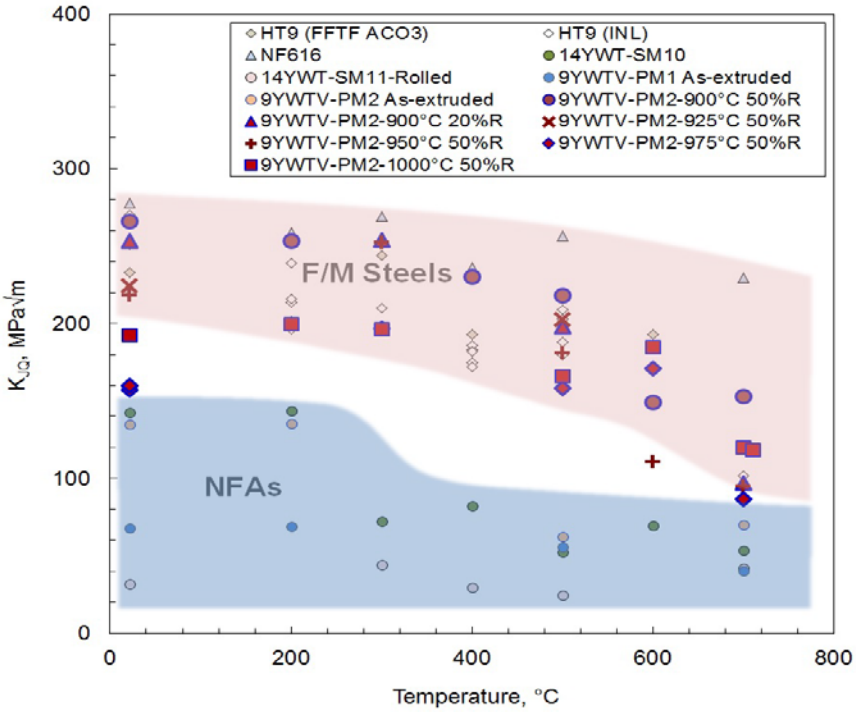


**Figure 9**. Temperature dependence in the fracture toughness ($K_{JQ}$) of 9YWTV-PM2 controlled rolled at various conditions. Data are compared with those of FM steels in pink (upper) shadowed area and those of lower toughness NFAs in blue (lower) shadowed area.

## SUMMARY

Fracture resistance behaviors have been characterized in detail for the newly developed 9YWTV alloys after various controlled rolling (CR) treatments.

Fracture resistance (J-R) tests have been carried out for the CR-treated 9YWTV-PM1 and 9YWTV-PM2 alloys over a wide temperature range of RT–700 °C and the data were analyzed using a simplified normalization method.

The fracture toughness of CR-treated 9YWTV-PM2 was as high as those of non-ODS F/M steels. In particular, the 9YWTV-PM2 controlled-rolled at 900°C demonstrated the best fracture toughness among NFAs, which were above 150 MPa√m over the entire test temperature range.

## Acknowledgement

This research was jointly sponsored by the Fuel Cycle R&D Program of the Office of Nuclear Energy, as well as by the Fusion Materials Program of Office of Fusion Energy, the U.S. Department of Energy, under Contract DE-AC05-00OR22725 with UT-Battelle, LLC. The authors express special thanks to Dr. Xiang Chen for his thorough review and thoughtful comments.

## REFERENCES

[1] S.J. Zinkle, G.S. Was, Acta Mater. 61 (2013) 735–758.
[2] B. Z. Margolin, A. I. Murashova, V. S. Neustroev, Strength of Mater. 44 (2012) 223-240.

[3] T.R. Allen, J.I Cole, C.L Trybus, D.L Porter, H. Tsai, F. Garner, E.A. Kenik, T. Yoshitake, J. Ohta, J. Nucl. Mater., 348 (2006) 148-164.
[4] I.I. Balachov, E.N. Shcherbakov, A.V. Kozlov, I.A. Portnykh, F.A. Garner, J. Nucl. Mater., 329–333 (2004) 617–620.
[5] S.A. Maloy, M. Toloczko, J. Cole, T.E. Byun, J. Nucl. Mater., 415 (2011) 302-305.
[6] V.S. Neustroev, F.A. Garner, J. Nucl. Mater., 386–388 (2009) 157–160.
[7] Y. Mutoh, K. Ichikawa, K. Nagata, M. Takeuchi, Journal of Materials Science, 30 (1995) 770–775.
[8] T.S. Byun, K. Farrell, J. Nucl. Mater., 318 (2003) 292-299.
[9] R.L. Klueh, D.R. Harris, High-chromium Ferritic and Martensitic Steels for Nuclear Applications, ASTM (2001), ISBN 0-803102090-7.
[10] T.R. Allen, J.T. Busby, R.L. Klueh, S.A. Maloy, M.B. Toloczko, JOM, 60 (2008) 15-23.
[11] R. Chaouadi, G. Coen, L. Lucon, V. Massaut, J. Nucl. Mater., 403 (2010) 15-18.
[12] T.S. Byun, M. Li, K. Farrell, Met. & Mat. Trans. A, 44 (2013) 84-93.
[13] S.A. Maloy, M. Toloczko, J. Cole, T.S. Byun, J. Nucl. Mater., 415 (2011) 302–305.
[14] J.S. Cheon, C.B. Lee, B.O. Lee, J.P. Raison, T. Mizuno, F. Delage, J. Carmack, J. Nucl. Mater., 392 (2009) 324-330.
[15] L. Tan, D.T. Hoelzer, J.T. Busby, M.A. Sokolov, R.L. Klueh, J. Nucl. Mater., 422 (2012) 45–50.
[16] J. Chen, M.A. Pouchon, A. Kimura, P. Jung, W. Hoffelner, J. Nucl. Mater., 386–388 (2009) 143–146.
[17] P. Lours, S. Le Roux, G. Bernhart, J. Adv. Mater., 33 (2001) 11-20.
[18] P. Krautwasser, A. Czyrska-Filemonowicz, M. Widera, F. Carsughi, Mater. Sci. Engi., A 177 (1994) 199-208.
[19] J. Chen, P. Jung, W. Hoffelner, H. Ullmaier, Acta Materialia, 56 (2008) 250–258.
[20] A Wasilkowska, M Bartsch, U Messerschmidt, R Herzog, A Czyrska-Filemonowicz, J. Mater. Process. Tech. (2003) 218-224.
[21] A. Czyrska-Filemonowicz, B. Dubiel, J. Mater. Process. Tech. 64 (1997) 53-64.
[22] T.S. Byun, J.H. Kim, J.H. Yoon, D.T. Hoelzer, J. of Nucl. Mater., 407 (2010) 78-82.
[23] R.L. Klueh, J.P. Shingledecker, R.W. Swindeman, D.T. Hoelzer, J. Nucl. Mater., 341 (2005) 103–114.
[24] M.B. Toloczko, D.S. Gelles, F.A. Garner, R.J. Kurtz, K. Abe, 329–333 (2004) 352–355.
[25] P. Miao, G.R. Odette, T. Yamamoto, M. Alinger, D. Klingensmith, J. Nucl. Mater., 377 (2008) 59–64.
[26] M.K. Miller, D.T. Hoelzer, E.A. Kenik, K.F. Russell, J. Nucl. Mater., 329–333 (2004) 338–341.
[27] D.T. Hoelzer, J. Bentley, M.A. Sokolov, M.K. Miller, G.R. Odette, M.J. Alinger, J. Nucl. Mater., 367-370 (2007) 166-172.
[28] M.J. Alinger, G.R. Odette, D.T. Hoelzer, Acta Mater., 57 (2009) 392-406.
[29] G.R. Odette, M.J. Alinger, B.D. Wirth, Ann. Rev. Mater., Res. 38 (2008) 471-503.
[30] M.K. Miller, D.T. Hoelzer, E.A. Kenik, K.F. Russell, Intermetallics 13 (2005) 387-392.
[31] S. Ukai, S. Ohtsuka, T. Kaito, H. Sakasegawa, N. Chikata, S. Hayashi, S. Ohnuki, Mater. Sci. Engi., A 510-511 (2009) 115-120.
[32] H. Sakasegawa, S. Ukai, M. Tamura, S. Ohtsuka, H. Tanigawa, H. Ogiwara, A. Kohyama, M. Fujiwara, J. Nucl. Mater., 373 (2008) 82–89.
[33] T.S. Byun, J.H. Yoon, D.T. Hoelzer, J. Nucl. Mater., (2012) in press.
[34] H.S. Cho, R. Kasada, A. Kimura, J. Nucl. Mater., 367 (2007) 239-243.
[35] H. Kishimoto, R. Kasada, O. Hashitomi, A. Kimura, J. Nucl. Mater., 386 (2009) 533-536.
[36] N. Akasaka, S. Yamashita, T. Yoshitake, S. Ukai, A. Kimura, J. Nucl. Mater., 329 (2004) 1053-1056.
[37] P. Olier, J. Malaplate, M.H. Mathon, D. Nunes, D. Hamona, L. Toualbi, Y. de Carlan, L. Chaffron, J. Nucl. Mater., 428 (2012) 40-46.
[38] S. Ukai, M. Harada, H. Okada, M. Inoue, S. Nomura, S. Shikakura, K. Asabe, T. Nishida, M. Fujiwara. J. Nucl. Mater., 204 (1993) 65-71.
[39] S. Ukai, T. Nishida, T. Okuda, T. Yoshitake, J. Nucl. Mater., 258 (1998) 1745-1749.
[40] A-L. Rouffié, P. Wident, L. Ziolek, F. Delabrouille, B. Tanguy, J. Crépin, A. Pineau, V. Garat, B. Fournier, J. Nucl. Mater., 433 (2013) 108–115.
[41] A. Steckmeyer, M. Praud, B. Fournier, J. Malaplate, J. Garnier, J.L. Béchade, I. Tournié, A. Tancray, A. Bougault, P. Bonnaillie, J. Nucl. Mater., 405 (2010) 95–100.

[42] J.H. Kim, J.H. Lee, J.Y. Min, S.W. Kim, C.H. Park, J.T. Yeom, T.S. Byun, J. Alloys and Compounds, (2013), in press.
[43] D.K. Mukhopadhyay, F.H. Froes, D.S. Gelles, J. Nucl. Mater., 258-263 (1998) 1209-1215.
[44] D.A. McClintock, D.T. Hoelzer, M.A. Sokolov, R.K. Nanstad, J. Nucl. Mater., 386 (2009) 307-311.
[45] D.A. McClintock, M.A. Sokolov, D.T. Hoelzer, R.K. Nanstad, J. Nucl. Mater., 392 (2009) 353-359.
[46] J.H. Kim, T.S. Byun, D.T. Hoelzer, J. of Nucl. Mater., 407 (2010) 143-150.
[47] J.H. Kim, T.S. Byun, D.T. Hoelzer, S.W. Kim, B.H. Lee, Mat. Sci. Eng. A, 559 (2013) 101-110.
[48] J.H. Kim, T.S. Byun, D.T. Hoelzer, C.H. Park, J.T. Yeom, J.K. Hong, Mat. Sci. Eng. A, 559 (2013) 111-118.
[49] J.H. Kim, T.S. Byun, D.T. Hoelzer, J. Nucl. Mater., 425 (2012) 147-155.